SAND77-1126
Unlimited Distribution

3157

MASTER

A ONE-DIMENSIONAL APPROXIMATE TECHNIQUE FOR EARTH PENETRATION CALCULATIONS*

P. Yarrington

Prepared by Sandia Laboratories, Albuquerque, New Mexico 87115
and Livermore, California 94550 for the United States Energy Research
and Development Administration under Contract AT (29-1)-789

September 1977

Sandia Laboratories

SF 2900 Q(7-73)

DISCLAIMER

Issued by Sandia Laboratories, operated for the United States Energy Research & Development Administration by Sandia Corporation.

Printed in the United States of America
Available from
National Technical Information Service
U. S. Department of Commerced
5285 Port Royal Road
Springfield, VA 22161
Price: Printed Copy $4.00; Microfiche $3.00

SAND77-1126
Unlimited Release

A ONE-DIMENSIONAL APPROXIMATE TECHNIQUE FOR EARTH PENETRATION CALCULATIONS*

by

P. Yarrington
Sandia Laboratories
Albuquerque, New Mexico 87115

ABSTRACT

The penetration process is approximated by the one-dimensional expansion of a cylindrical cavity in an infinite solid. We use linear and quadratic forms to describe, piecewise, the volumetric response of the target during loading at the shock front, and assume that the density locks at the shocked state. The shear strength of the target is taken to be a piecewise linear function of pressure. However, it is assumed that the target material is weak in shear and, thus, that the effect of shear strength can be treated as a perturbation on the hydrodynamic solution. For conical-nosed penetrators an analytic expression for the normal stress results from the analysis, while for ogival-nosed penetrators the solution must be obtained numerically. A computer program, PENAP, was written to treat both the ogive and cone geometry, and PENAP solutions were found to agree well with both experimental data and TOODY, two-dimensional finite-difference wavecode results. It should also be noted that the PENAP calculations typically required several orders of magnitude less computer time than did the TOODY calculations.

*This work is supported by the U. S. Energy Research and Development Administration.

CONTENTS

FIGURES

I. INTRODUCTION

This report presents an approximate method for calculating the distribution of normal stress on conical- and ogival-nosed earth penetrators. The principal assumptions made in developing this technique were that (1) the penetration is at all times an axisymmetric event, (2) the penetrator can be treated as a rigid body, (3) motion of the target material is strictly one-dimensional (and radial) and (4) elastic strains in the target are negligibly small compared with total strains.

Justification for these assumptions, along with a discussion of the restrictions which they place on the applicability of the approximate technique, is presented in Section II. In Section III, it is shown that with these assumptions the equations of mass and momentum balance yield an integral expression for the time-dependent radial component of surface traction on the penetrator. In order to evaluate this expression, it is necessary to make constitutive assumptions for the hydrostatic response and shear strength of (or failure surface for) the target. Specific forms for the hydrostat and failure surface are assumed in Section IV, and assumption (4) is invoked permitting the effects of the target's shear strength to be treated as a perturbation on the hydrodynamic solution.

The special case of a conical-nosed penetrator is treated in Section V, where it is shown that, for this case, the successive equations of Section IV can be integrated in closed form, yielding an analytic expression for the boundary traction. In general, however, the integrations must be done numerically, and a computer program, PENAP [1], was written to perform those calculations for both ogival- and conical-nosed penetrators.

In Section VI, surface traction distributions calculated with PENAP (and with the equations of Section V, for conical-nosed penetrators) are compared with those obtained from two-dimensional, Lagrangian, finite-difference calculations made with the wavecode TOODY [2,3]. In the TOODY calculations, the elastic-plastic soil-cap model [4,5] was used to describe the constitutive response of the target. From the calculated surface tractions, the total axial force on the penetrator, hence its deceleration, can be computed, and presented in Section VI is a comparison of calculated and measured deceleration data for one of the Watching Hill penetration tests.

It should be noted that computation time for the PENAP calculations was typically several order of magnitude less than that required for the TOODY calculations. Furthermore, the interactive nature of the PENAP code and the simplicity of the material model used in the approximate techniques made the problem setup for PENAP calculations much more convenient than that for TOODY.

II. PRINCIPAL ASSUMPTIONS

As mentioned in the introduction, the four principal assumptions (apart from specific constitutive equations) made in developing this approximate technique were: (1) the penetration is at all times an axisymmetric event, (2) the penetrator can be treated as a rigid body, (3) motion of the target material is strictly one-dimensional (and radial) and (4) elastic strains in the target are negligibly small compared with total strains.

Clearly, assumption (1) restricts the applicability of the present analysis to the case of normal impact, i.e., when both the impact angle and angle of attack of the penetrator are zero. Since axisymmetric forms of the governing equations are chosen at the outset, it is not possible that the results of this analysis could be used, directly, for other than axisymmetric penetration problems.

Assumption (2) implies that deformations of the penetrator and the target can be uncoupled during the penetration event. That this assumption does not introduce significant error in boundary load calculations has been shown in [6] from TOODY calculations for a particular soil target and steel penetrator.

Assumption (3) is equivalent to assuming that displacement of target particles in the direction of penetrator motion (i.e., their axial displacement) is small compared with their displacement normal to the penetrator's axis (i.e., their radial displacement). Thus, the present technique would be expected to yield better approximations to the actual boundary traction for slender penetrators. It has been found, however, from TOODY soil penetration calculations in which penetrator-target interfacial friction was included, that the higher axial velocities induced

in the target by frictional forces did not significantly alter the normal stress distribution on the penetrator. This can be explained by the fact that, in general, soils are weak in shear and, thus, during a penetration event when motion of target particles is primarily in the radial direction, even relatively low particle velocities in the axial direction cause the material to yield plastically. Increasing the shear strain through an increase in axial particle velocity will, then, have little effect on the state of stress in the soil. The implication of this for the approximate technique is that better results might be obtained for more blunt penetrators than would be expected with assumption (3).

It is assumed that at the shock front, which propagates radially from the surface of the penetrator, the material is yielding plastically but can reach any state consistent with its hydrostat and failure surface. Furthermore, the density is assumed to remain constant after the shock passes, and, in particular, during unloading there is no recovery of elastic strains, consistent with assumption (4). This model (called the "plastic gas" model by Rakhmatulin and Stepanova, see [7]) is similar to earlier locking solid models (see, e.g., [8], [9], or [10]); however, in the present case, the material is not restricted to lock at any particular density as in the earlier models.

This is felt to provide a better description of the target response during penetration, and clearly provides a less restrictive constitutive model for the material response. However, these constitutive assumptions will only be reasonable for highly hysteretic, non-dilatant materials with relatively low shear strength. Experimental evidence (see, e.g., [11]) suggests that most loose soils are of this sort, while more dense or cohesive geologic media (and, in particular, most competent rock) are not.

III. BASIC EQUATIONS

We will approximate the penetration process by the one-dimensional expansion of a cylindrical cavity in an infinite solid. The radius of the cavity is assumed to be a prescribed function of time, $R(t)$, corresponding to the radial displacement which the target material adjacent to the penetrator must have to stay on the surface of the penetrator. We will then interpret the internal pressure, $p(t)$, necessary to expand the cavity according to $R(t)$, as the radial component of normal traction on the penetrator.

For one-dimensional, cylindrically symmetrical motion of a continuum, the local equations of momentum and mass conservation in cylindrical Lagrangian coordinates (r, θ, z) reduce to:

$$\rho_o r \frac{\partial^2 u}{\partial t^2} = -(r + u) \frac{\partial \sigma_r}{\partial r} - (\sigma_r - \sigma_\theta) \frac{\partial}{\partial r} (r + u) \quad , \tag{3.1}$$

and

$$\frac{\partial}{\partial r} (r + u)^2 = 2 \frac{\rho_o}{\rho} r \quad , \tag{3.2}$$

where ρ_o is the reference density, ρ is the current density, u is the radial displacement, and σ_r and σ_θ are the radial and circumferential components of Cauchy stress, respectively, both taken to be positive in compression. All field quantities are assumed to be functions of the radial coordinate, r, and time, t, unless otherwise indicated.

We assume that elastic strains in the material are negligible and that during loading: (1) the material is yielding plastically, with

$$\sigma_r - \sigma_\theta = \tau_o + \mu\sigma \, , \quad \sigma_r = \sigma_z \quad , \tag{3.3}$$

where σ_z is the axial component of stress and $\sigma = \frac{1}{3}(\sigma_r + \sigma_\theta + \sigma_z)$ is the hydrostatic pressure, and (2) the pressure and volumetric strain are related through an equation of the form

$$\sigma = f\left(1 - \frac{\rho_o}{\rho}\right) \quad . \tag{3.4}$$

With (3.3), setting $\upsilon \equiv 3\mu/(3 + \mu)$ and multiplying both sides of (3.1) by $(r + u)^{\upsilon-1}$, (3.1) can be written as

$$\frac{\partial}{\partial r}\left[(r + u)^{\upsilon}\sigma_r\right] = -\rho_o r(r + u)^{\upsilon-1}\frac{\partial^2 u}{\partial t^2} - \tau_o\left(\frac{\upsilon}{\mu}\right)(r + u)^{\upsilon-1}\frac{\partial}{\partial r}(r + u) \quad . \tag{3.5}$$

We assume that at $t = 0$, $R(t) = 0$ and the cavity begins expanding, suddenly, sending a shock wave into the material. Letting $h(t)$ be the position of the shock front, then formally integrating (3.5) with respect to r yields

$$(r + u)^{\nu}\sigma_r = -\rho_o\int_0^r (\hat{r} + u)^{\nu-1}\hat{r}\frac{\partial^2 u}{\partial t^2}\,d\hat{r}$$

$$- \frac{\tau_o}{\mu}\left[(r + u)^{\nu} - R^{\nu}\right] + R^{\nu}p \, , \quad 0 \le r \le h \quad , \tag{3.6}$$

where $p = p(t) = \sigma_r(0, t)$ is the internal pressure on the cavity wall. For the special case in which $\mu \equiv 0$, the integration yields

$$\sigma_r = -\rho_o \int_0^r \frac{\hat{r}}{\hat{r} + u} \frac{\partial^2 u}{\partial t^2} d\hat{r} - \tau_o[\ell n(r + u) - \ell nR] + p \quad ,$$

$$0 \leq r \leq h \quad . \tag{3.7}$$

As indicated, the relations (3.6) and (3.7) hold for all values of r between the cavity wall, r = 0, and the shock front, r = h. Evaluating at r = h, and letting an asterisk denote the value of a function immediately behind the shock front, we get from (3.6)

$$R^\nu p = \rho_o \int_0^h (\hat{r} + u)^{\nu-1} \hat{r} \frac{\partial^2 u}{\partial t^2} d\hat{r} + \frac{\tau_o}{\mu}(h^\nu - R^\nu) + h^\nu \sigma_r^* \quad , \tag{3.8}$$

and from (3.7)

$$p = \rho_o \int_0^h \frac{\hat{r}}{\hat{r} + u} \frac{\partial^2 u}{\partial t^2} d\hat{r} + \tau_o \ell n \left(\frac{h}{R}\right) + \sigma_r^* \quad . \tag{3.9}$$

We make one further assumption, namely, that at any point in the material, the density "locks" immediately behind the shock front. Thus, behind the shock the density will be a function of r, only. With that assumption, (3.9) can be formally integrated with respect to r yielding

$$(r + u)^2 = 2 \int_0^r \frac{\rho_o}{\rho(\hat{r})} \hat{r} d\hat{r} + f(t) \quad , \quad 0 \leq r \leq h \quad . \tag{3.10}$$

With the condition

$$u(0, t) = R(t) \quad ,$$

we see from (3.10) that

$$f(t) = R^2(t) \quad .$$

Thus, setting

$$\psi(r) = \int_0^r \frac{\rho_o}{\rho(\hat{r})} \hat{r} d\hat{r} \quad , \tag{3.11}$$

(3.10) becomes

$$(r + u)^2 = 2\psi(r) + R^2(t) \quad . \tag{3.12}$$

From (3.12) it follows that

$$\dot{u} \equiv \frac{\partial u}{\partial t} = \frac{R\dot{R}}{(2\psi + R^2)^{1/2}} \quad , \tag{3.13}$$

and

$$\ddot{u} \equiv \frac{\partial^2 u}{\partial t^2} = \frac{\dot{R}^2 + R\ddot{R}}{(2\psi + R^2)^{1/2}} - \frac{(R\dot{R})^2}{(2\psi + R^2)^{3/2}} \quad . \tag{3.14}$$

Evaluating (3.12) at r = h

$$h^2 = 2\psi(h) + R^2 \quad . \tag{3.15}$$

Furthermore, at the shock front, the jump conditions

$$\rho_o \dot{h} = \rho^* \dot{h} - \rho^* \dot{u}^* \quad , \tag{3.16}$$

and

$$\sigma_r^* = \rho_o \dot{h} \dot{u}^* \quad , \tag{3.17}$$

must be satisfied.

Differentiating (3.15) with respect to time, and recalling (3.11), we get

$$\dot{h\eta} = \frac{\rho_o}{\rho^*}\dot{h\eta} + R\dot{R} \quad ,$$

or, letting

$$\eta = 1 - \frac{\rho_o}{\rho} \quad , \tag{3.18}$$

we have

$$\dot{h\eta}^* = R\dot{R} \quad . \tag{3.19}$$

From (3.3) and (3.4)

$$\sigma_r = \left(\frac{3+\mu}{3}\right) f(\eta) + \frac{\tau_o}{3} \quad , \tag{3.20}$$

and eliminating $\dot{u}^*$ between (3.16) and (3.17), and using (3.20) it follows that

$$\rho_o \dot{h}^2 \eta^* = \sigma_r^* = \left(\frac{3+\mu}{3}\right) f(\eta^*) + \frac{\tau_o}{3} \quad . \tag{3.21}$$

Assuming that $f(\eta)$ is such that (3.21) can be solved for η^*, then we can write

$$\eta^* = g(\dot{h}) \quad , \tag{3.22}$$

and (3.19) becomes

$$\dot{h}g(\dot{h}) = R\dot{R} \quad . \tag{3.23}$$

Thus, for a prescribed displacement $R(t)$ at the cavity, (3.23) yields the position of the shock front in the material as a function of time, from which η^* can be found through (3.22). Since the density at a

material point changes only as the shock front passes, then if $\tilde{r} = h(\tilde{t})$, we can write

$$\eta(\tilde{r}, t) = \eta(\tilde{r}) = \begin{cases} \eta^*(\tilde{t}), & t \geq \tilde{t} \\ 0, & t < \tilde{t} \end{cases} , \tag{3.24}$$

and (3.11) becomes

$$\psi(r) = \int_0^r [1 - \eta(\hat{r})] \hat{r} d\hat{r} . \tag{3.25}$$

Finally, with (3.25) we can evaluate (3.13) and (3.14), and solve (3.8) for the cavity pressure p. From (3.19) and (3.21) it is clear that, in general, a coupled set of nonlinear, first-order differential equations must be solved for the functions η^* and h.

IV. PERTURBATION ANALYSIS FOR LOW STRENGTH TARGETS

We assume that the volumetric response of soils can be described by

$$\sigma = \begin{cases} K_1 \eta \ , & 0 \le \eta \le \eta_1 \le 1 \ , \\ K_2 \eta^2 \ , & \eta_1 \le \eta \le \eta_2 \le 1 \ , \end{cases} \tag{4.1}$$

while the yield condition can be approximated by

$$\tau = \begin{cases} \mu\sigma \ , & 0 \le \sigma \le \sigma_1 \ , \\ \tau_o \ , & \sigma_1 \le \sigma \ , \end{cases} \tag{4.2}$$

where τ is the maximum principal stress difference. From (4.1) and (4.2) we see that, at any particular time, the response of the soil at a given point is determined by the equations for one of the following cases:

$$\begin{aligned} &\text{Case 1.} && \sigma = K_1 \eta \ , && \tau = \tau_o \ , \\ &\text{Case 2.} && \sigma = K_2 \eta^2 \ , && \tau = \tau_o \ , \\ &\text{Case 3.} && \sigma = K_1 \eta \ , && \tau = \mu\sigma \ , \\ &\text{Case 4.} && \sigma = K_2 \eta^2 \ , && \tau = \mu\sigma \ . \end{aligned} \tag{4.3}$$

We distinguish soils from other geologic media (or other materials for which (4.1) and (4.2) may apply) by the condition that they be weak in shear, in the sense that

$$\frac{\tau}{K_i} \ll 1 \ . \tag{4.4}$$

Considering (4.4) we will treat the effect of shear strength as a perturbation on the hydrodynamic case, for which $\tau \equiv 0$. Taking the perturbation parameter, ε, to be given by

$$\varepsilon = \frac{\tau_o}{3K_i} \quad , \tag{4.5}$$

we assume the expansions

$$\begin{aligned} \eta &= \eta_o + \varepsilon\eta_1 + \cdots \quad , \\ h &= h_o + \varepsilon h_1 + \cdots \quad . \end{aligned} \tag{4.6}$$

With the relations $(4.3)_1$ for Case 1, (3.21) becomes

$$\rho_o \dot{h}^2 \eta^* = K_1 \eta^* + \frac{\tau_o}{3} \quad , \tag{4.7}$$

where for this case, $\mu = 0$. Substituting the expansions (4.6) in (4.7) and (3.19), and collecting coefficients of like powers in ε, we find that through first-order terms,

$$\dot{h}_o = \left(\frac{K_1}{\rho_o} \right)^{1/2} \quad , \tag{4.8}$$

$$\dot{h}_1 = \frac{1}{2} \left(\frac{K_1}{\rho_o} \right)^{3/2} \frac{t}{R\dot{R}} \quad , \tag{4.9}$$

$$\eta_o^* = \frac{\rho_o}{K_1} \frac{R\dot{R}}{t} \quad , \tag{4.10}$$

$$\eta_1^* = -\left(\frac{\dot{h}_1}{\dot{h}_o} + \frac{h_1}{h_o} \right) \eta_o^* \quad . \tag{4.11}$$

For Case 2, in which $(4.3)_2$ applies, the above procedure yields the successive equations:

$$h_o \dot{h}_o^3 = \frac{K_2}{\rho_o} R\dot{R} \quad , \tag{4.12}$$

$$\dot{h}_1 + \frac{1}{3} \frac{\dot{h}_o}{h_o} h_1 = \frac{1}{3} \left(\frac{K_2}{\rho_o} \right) \frac{1}{\dot{h}_o^2} \quad , \tag{4.13}$$

$$\eta_o^* = \frac{\rho_o}{K_2} \dot{h}_o^2 \quad , \tag{4.14}$$

$$\eta_1^* = 2 \frac{\rho_o}{K_2} \dot{h}_o \dot{h}_1 - \frac{1}{\eta_o^*} \quad . \tag{4.15}$$

From (3.21), $(4.3)_3$ and $(4.3)_4$, we see that Cases 3 and 4 correspond to Cases 1 and 2, respectively, with $\tau_o \equiv 0$ and the bulk moduli K_i $(i = 1, 2)$ multiplied by the constant: $(3 + \mu)/3$. Notice that, since we have $\tau_o \equiv 0$, a perturbation analysis for Cases 3 and 4 is unnecessary, and in fact, we can write down equations for obtaining the exact solutions (for η^* and h) for these cases from the zeroth-order equations for Cases 1 and 2. Accordingly, from (4.8) and (4.10), we have for Case 3

$$\dot{h} = \left(\frac{3 + \mu}{3} \right)^{1/2} \left(\frac{K_1}{\rho_o} \right)^{1/2} \quad , \tag{4.16}$$

$$\eta^* = \frac{\rho_o}{K_1} \left(\frac{3}{3 + \mu} \right) \frac{R\dot{R}}{t} \quad , \tag{4.17}$$

while, from (4.12) and (4.14), we have for Case 4

$$h\dot{h}^3 = \frac{K_2}{\rho_o}\left(\frac{3+\mu}{3}\right) R\dot{R} \quad , \tag{4.18}$$

$$\eta^* = \frac{\rho_o}{K_2}\left(\frac{3}{3+\mu}\right) \dot{h}^2 \quad . \tag{4.19}$$

It can be seen from (4.8)-(4.15) that, while the nonlinear character of the equations to be solved has not changed, the perturbation analysis together with the constitutive assumptions has uncoupled the equations in terms of their dependence on the functions η^* and h. As will be seen below, the uncoupling of the equations permits the use of fairly direct methods for their solution.

V. SPECIAL CASE: CONICAL-NOSED PENETRATOR

We consider, here, the special case in which the penetrator nose shape is conical. In this case, R(t) is given by

$$R = Vt \quad , \tag{5.1}$$

where V is a constant, proportional to the velocity of the penetrator. In particular, if the nose is of length L and diameter D, and the velocity of the penetrator is V_o, then $V = \frac{D}{2L} V_o$.

For the conical nose shape, we will solve (4.12)-(4.15) for Case 2, and, using those results, obtain an approximate solution for the boundary pressure from (3.9). For the sake of completeness, we will also present the results for Cases 1, 3 and 4; however, details of the solutions will be omitted.

With (5.1) and the condition that

$$h(0) = 0 \quad , \tag{5.2}$$

(4.12) can be integrated yielding

$$h_o = \left(\frac{K_2}{\rho_o}\right)^{1/4} V^{1/2} t \quad . \tag{5.3}$$

Using (5.2) and (5.3), (4.13) has the solution

$$h_1 = \frac{1}{4}\left(\frac{K_2}{\rho_o}\right)^{5/4} V^{-3/2} t \quad . \tag{5.4}$$

Thus, with (5.3) and (5.4), (4.14) and (4.15) become

$$\eta_o^* = \left(\frac{\rho_o V^2}{K_2} \right)^{1/2} , \tag{5.5}$$

$$\eta_1^* = -\frac{1}{2} \left(\frac{\rho_o V^2}{K_2} \right)^{-1/2} . \tag{5.6}$$

To first order in ε, then, we see from (4.6) that η^* is a constant given by

$$\eta^* = \eta_o^* + \varepsilon \eta_1^* = \left(\frac{\rho_o V^2}{K_2} \right)^{1/2} - \frac{\varepsilon}{2} \left(\frac{\rho_o V^2}{K_2} \right)^{-1/2} , \tag{5.7}$$

where the perturbation parameter ε is defined by (4.5).

Recall that for the constitutive model we are using, η changes only at the shock front, i.e., (3.24) holds. Thus, we see from (5.7) that the density of the material between the cavity and the shock front must be a constant, determined by (5.7) through

$$\frac{\rho_o}{\rho} = 1 - \eta = 1 - \eta^* . \tag{5.8}$$

Using (5.8) in (3.25), we get

$$\psi(r) = \frac{1}{2} b r^2 , \tag{5.9}$$

where

$$b = 1 - \eta^* . \tag{5.10}$$

It follows from (3.12), (3.14) and (5.9) that (3.9) becomes

$$p = \rho_o \int_0^h \frac{r\dot{R}^2}{br^2 + R^2}\, dr - \rho_o \int_0^h \frac{r(R\dot{R})^2}{(br^2 + R^2)^2}\, dr$$

$$+ \tau_o \ell n\left(\frac{h}{R}\right) + \sigma_r^* \quad . \tag{5.11}$$

Integrating (5.11), and simplifying the result, we get

$$p = \frac{\rho_o R^2}{2b} \ell n\left[b\left(\frac{h}{R}\right)^2 + 1\right] - \frac{\rho_o \dot{R}^2}{2} \frac{h^2}{bh^2 + R^2} + \tau_o \ell n\left(\frac{h}{R}\right) + \sigma_r^* \quad . \tag{5.12}$$

With (5.10), (3.19) becomes

$$h\dot{h}(1 - b) = R\dot{R} \quad ,$$

or

$$\dot{h}^2 = \frac{(R\dot{R})^2}{h^2(1 - b)^2} \quad . \tag{5.13}$$

Evaluating (5.9) at r = h, and using that result in (3.15) we find that

$$h^2 = \frac{R^2}{1 - b} \quad . \tag{5.14}$$

Substituting (5.14) in (5.13), gives the result

$$\dot{h}^2 = \frac{\dot{R}^2}{1 - b} \quad , \tag{5.15}$$

and using (5.15), together with (5.10), in the first equality of (3.21),

we get

$$\sigma_r^* = \rho_o \dot{R}^2 \quad . \tag{5.16}$$

With (5.1), (5.14) and (5.16), (5.12) reduces to

$$p = \frac{\rho_o V^2}{2} \left[1 - \frac{\ell n(1-b)}{b} \right] - \frac{1}{2} \tau_o \ell n (1-b) \quad . \tag{5.17}$$

For Case 1, the successive equations (4.8)-(4.11) apply, and an analysis similar to that presented above has the results

$$h = h_o + \varepsilon h_1 = \left(\frac{K_1}{\rho_o} \right)^{1/2} t + \frac{1}{2} \varepsilon \left(\frac{K_1}{\rho_o} \right)^{3/2} V^{-2} t \quad , \tag{5.18}$$

$$\eta^* = \eta_o^* + \varepsilon \eta_1^* = \frac{\rho_o}{K_1} V^2 - \varepsilon \quad . \tag{5.19}$$

Again, it is seen from (5.19) that the density jump at the shock front is a constant. Thus, (5.8) - (5.17) hold for this case, also, with

$$b = 1 - \eta^* = 1 - \frac{\rho_o}{K_1} V^2 + \varepsilon \quad . \tag{5.20}$$

Comparing (4.16) and (4.17) for Case 3 with (4.8) and (4.10) for Case 1, we see that these equations are of the same form. In fact, the solution for the set (4.16) and (4.17) differs from that for (4.8) and (4.10) only in that the bulk modulus, K_1, in the Case 1 solutions must be multiplied by the constant $(3 + \mu)/3$ for the Case 3 solutions.

Thus, considering (5.18) and (5.19), we have for Case 3:

$$h = \left(\frac{3 + \mu}{3} \right)^{1/2} \left(\frac{K_1}{\rho_o} \right)^{1/2} , \tag{5.21}$$

$$\eta^* = \left(\frac{3}{3 + \mu} \right) \frac{\rho_o}{K_1} V^2 . \tag{5.22}$$

Finally, comparing (4.18) and (4.19) for Case 4 with (4.12) and (4.14) for Case 2, we see, again, that the two sets of equations are identical except for the constant $(3 + \mu)/3$ multiplying the bulk modulus, K_2. Thus, we can write down immediately, from (5.3) and (5.5), the solutions for Case 4:

$$h = \left(\frac{3 + \mu}{3} \right)^{1/4} \left(\frac{K_2}{\rho_o} \right)^{1/4} V^{1/2} t , \tag{5.23}$$

$$\eta^* = \left(\frac{3}{3 + \mu} \right)^{1/2} \left(\frac{\rho_o V^2}{K_2} \right)^{1/2} . \tag{5.24}$$

Since by (5.22) and (5.24) we see that η^* is constant for both Cases 3 and 4, the results (5.8) - (5.10) and (5.13) - (5.15) are valid for these cases, also. Using those results in (3.8), and recalling that $\tau_o \equiv 0$ for Cases 3 and 4, it can be shown that (3.8) reduces to

$$p = \frac{\rho_o V^2}{b\nu(\nu - 2)} [(b\nu - 2)(1 - b)^{-\nu/2} + 2] + \rho_o V^2 (1 - b)^{-\nu/2} , \tag{5.25}$$

where $\nu \equiv 3\mu/(3 + \mu)$.

As mentioned in Section 3, we interpret the cavity pressure, p, given for the cone by either (5.17) or (5.25), as the radial component of the normal stress on the penetrator. Thus, if θ is the half-angle of the conical nose $\left(\text{i.e., } \theta = \text{Tan}^{-1}\left[\frac{2L}{D}\right]\right)$, then

$$\sigma_N = p/\cos\theta \quad . \tag{5.26}$$

Finally, it should be noted that, in general, it is not obvious which of the cases specified in (4.3) should be used for a particular penetration problem. It becomes necessary, then, to calculate n^* for each case and check the result against the limits in (4.1) and (4.2). (This checking is done automatically in the PENAP [1] code.)

VI. COMPARISON WITH TOODY RESULTS AND EXPERIMENTAL DATA

The equations of the approximate analysis presented in Sections 3 and 4 were incorporated in an interactive NOS computer code, PENAP [1], which calculates normal stress distributions and deceleration histories for both conical- and ogival-nosed penetrators. In this section, we will compare PENAP solutions with TOODY [2,3] two-dimensional, finite-difference results and with data from the Watching Hill series of penetration experiments. For the TOODY calculations the soil-cap model [3,4] was used to describe target material response.

For three soils, cap model parameters have been determined which provide a reasonably close fit to quasi-static data (see, [12]). These parameters were used in [12] to model the first three soil layers at the Watching Hill site. The hydrostat and failure envelope generated by the cap model for these layers are shown in Figs. 1-3. Included in the figures are the curves which were used for the approximate calculations. Notice that, as assumed in (4.1) and (4.2), the approximate curves use a linear-quadratic fit to the hydrostat and a linear-constant fit to the failure envelope, or yield condition.

a. Normal Stress Distributions

For the purpose of comparing TOODY calculations of normal stress distribution with those of the approximate method, Layers 1 and 3 were chosen as targets. The TOODY calculations were run with initially square zones of 15 mm, while for the PENAP calculations, the time required for one nose length of penetration (at the impact velocity) was partitioned into 200 equal increments, and this partition was used for the numerical

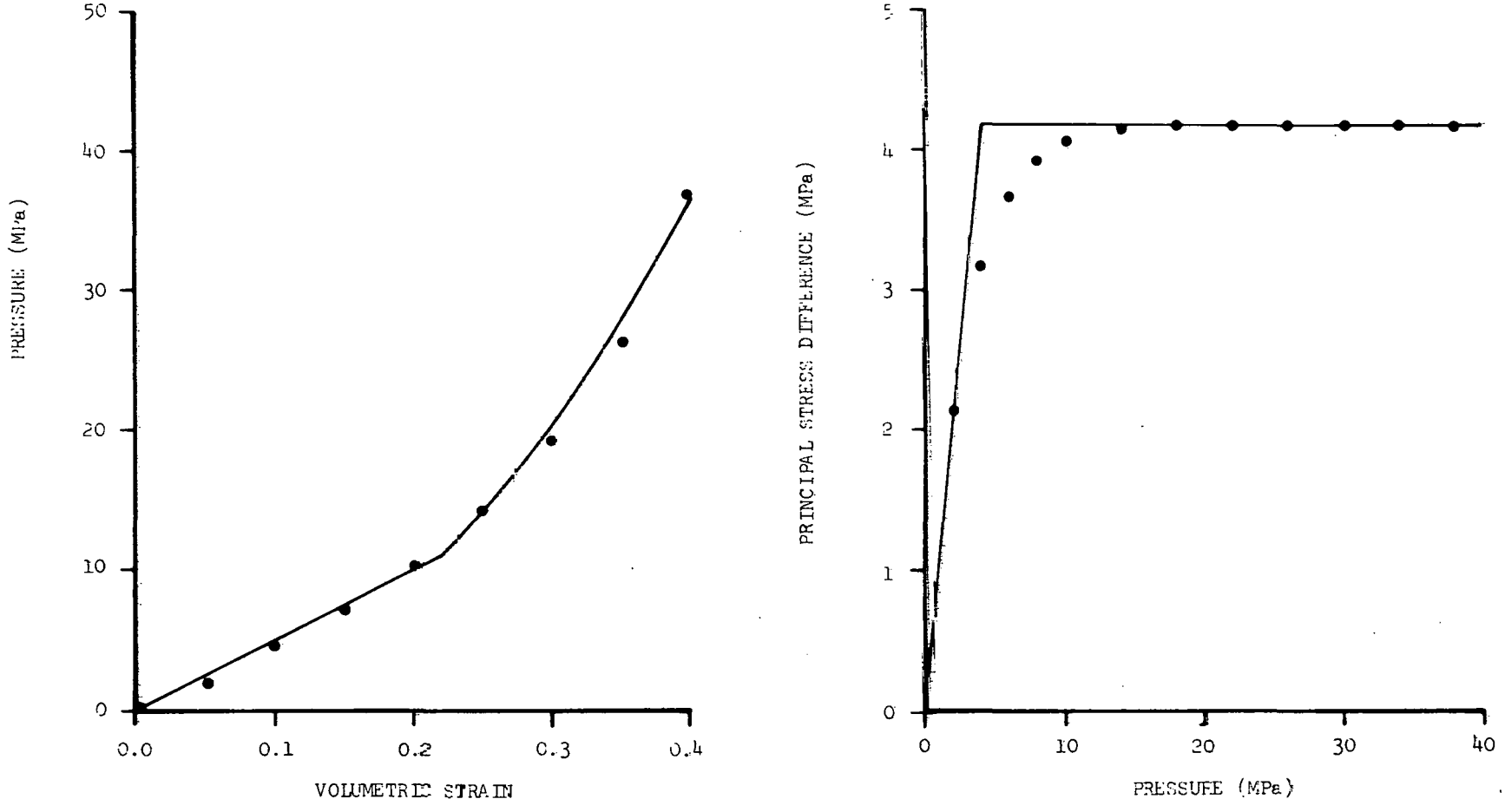

Figure 1. Hydrostat and Failure Surface for Layer 1
Cap Model • • •
Approximate Fit ——

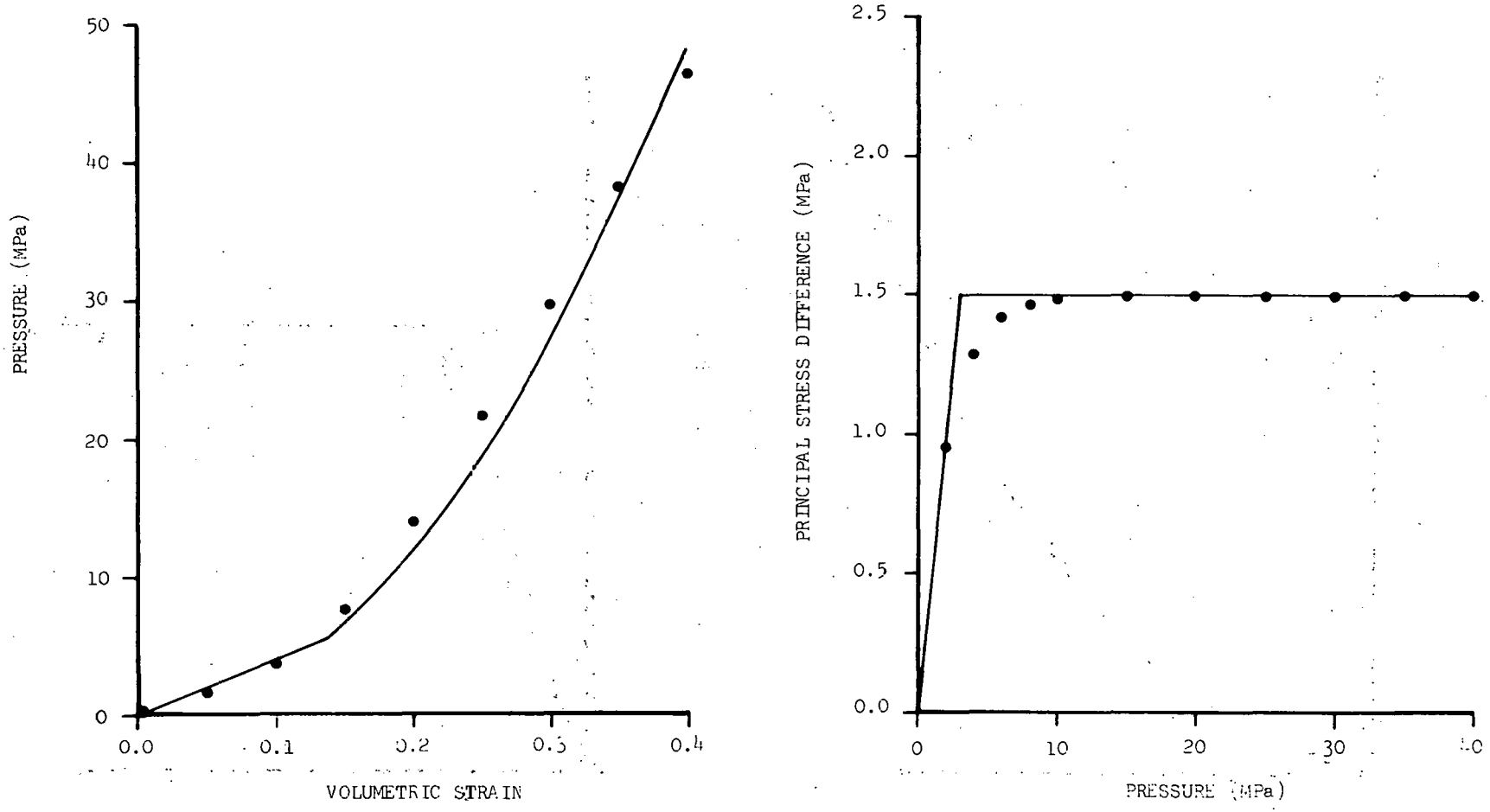

Figure 2. Hydrostat and Failure Surface for Layer 2
Cap Model • • •
Approximate Fit ——

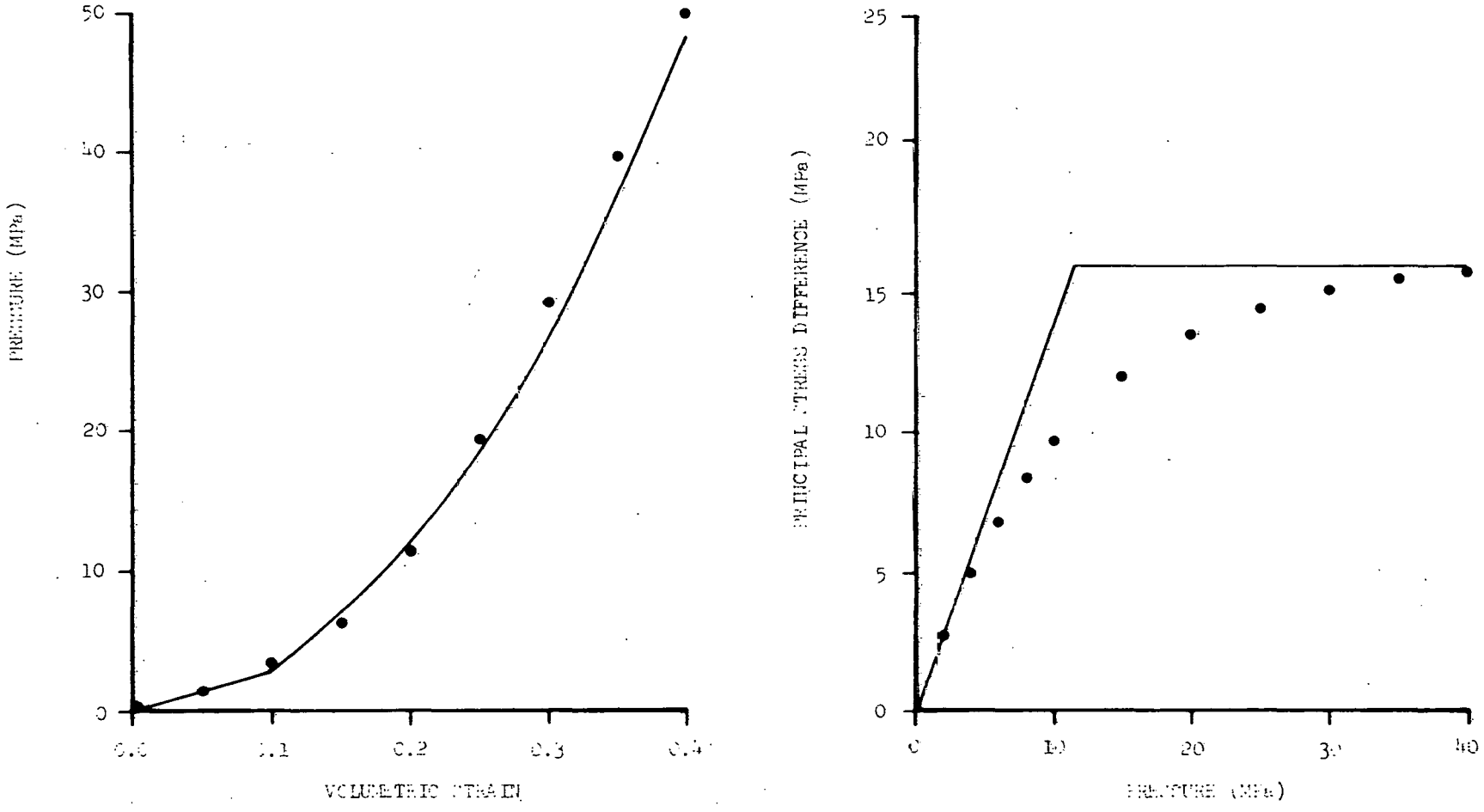

Figure 3. Hydrostat and Failure Surface for Layer 3
Cap Model • • •
Approximate Fit ———

integrations. In calculating the normal stress at a point on the penetrator, TOODY interpolates stresses in the calculational grid to the normal line at that point and then extrapolates the normal component of stress to the penetrator boundary (see, [12]). In the PENAP calculations, the cavity pressure found from (3.8) or (3.9) is interpreted as the radial component of the normal stress on the penetrator.

An initial test calculation was made for a conical-nosed ($L/D = 3.0$) penetrator impacting Layer 1 at 500 m/s. Since, as was seen in Section 5, the present approximate method yields an analytic expression for the (spatially constant) normal stress on a conical nose, this case provides a convenient check on the PENAP numerical scheme. The PENAP results, along with the normal stress calculated using the equations of Section 5 (viz., (5.17), together with (5.20) and 5.26)) are shown in Fig. 4.

Calculations were made with TOODY and PENAP for a 9.25 caliber ogival-nosed penetrator taking Layers 1 and 3 as targets (initial densities: Layer 1, 1.490 Mg/m^3; Layer 3, 1.859 Mg/m^3). Two impact velocities were considered for each layer, namely, 75 m/s and 150 m/s for Layer 3 and 150 m/s and 500 m/s for Layer 1. The normal stress distributions calculated with TOODY and PENAP are compared in Figs. 5-8.

Considering the simplicity of the approximate theory, compared with the two-dimensional kinematics and soil-cap model used for the TOODY solutions, the comparison between TOODY and PENAP results is quite good. Furthermore, the fact that both the kinematics and the constitutive model used in the approximate method are different from that used in TOODY makes it difficult to identify the source of relatively small discrepancies between the two solutions.

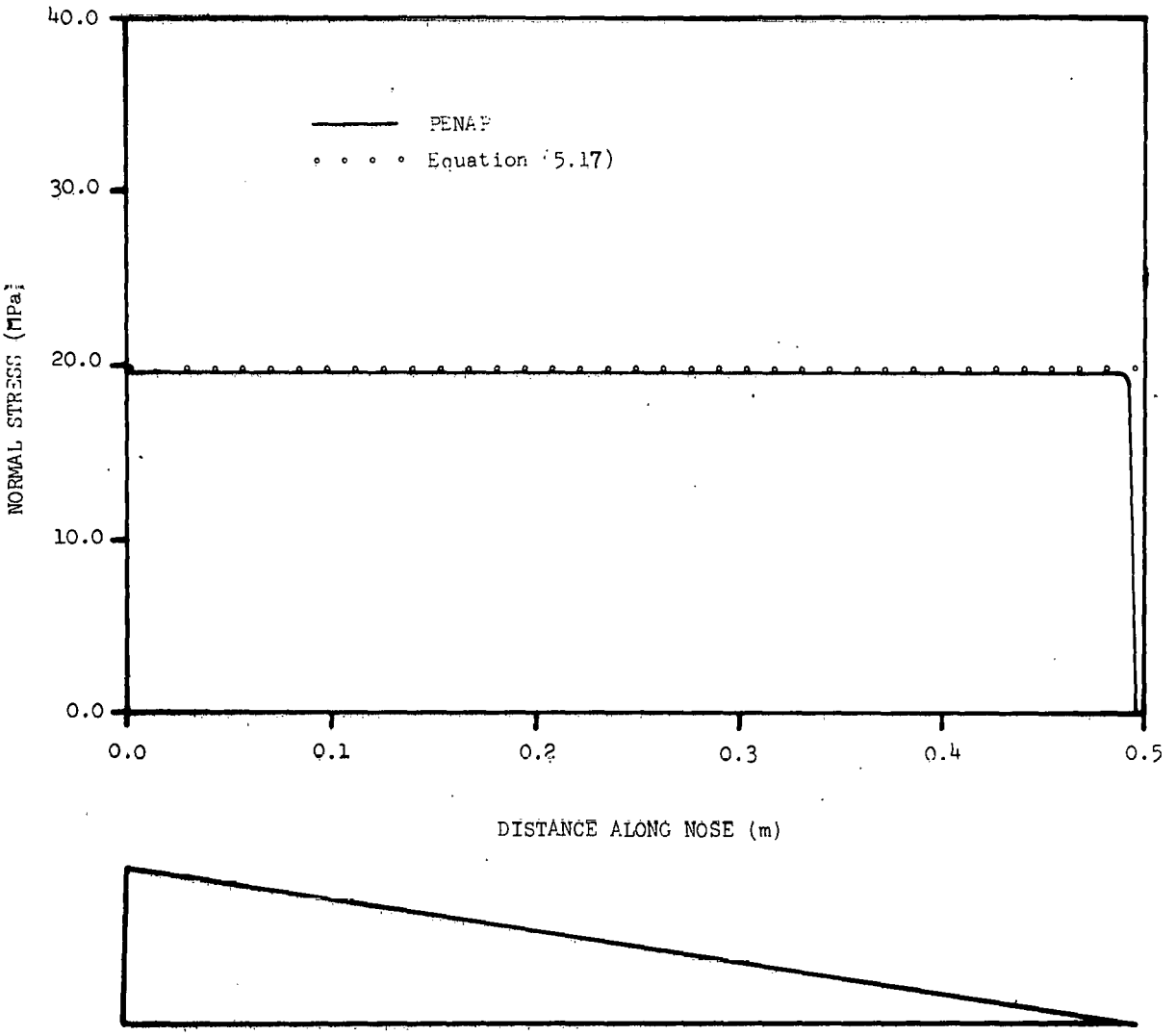

Figure 4. Normal Stress Distribution on Conical-Nosed Penetrator (Target: Layer 1; Impact Velocity: 500 m/s)

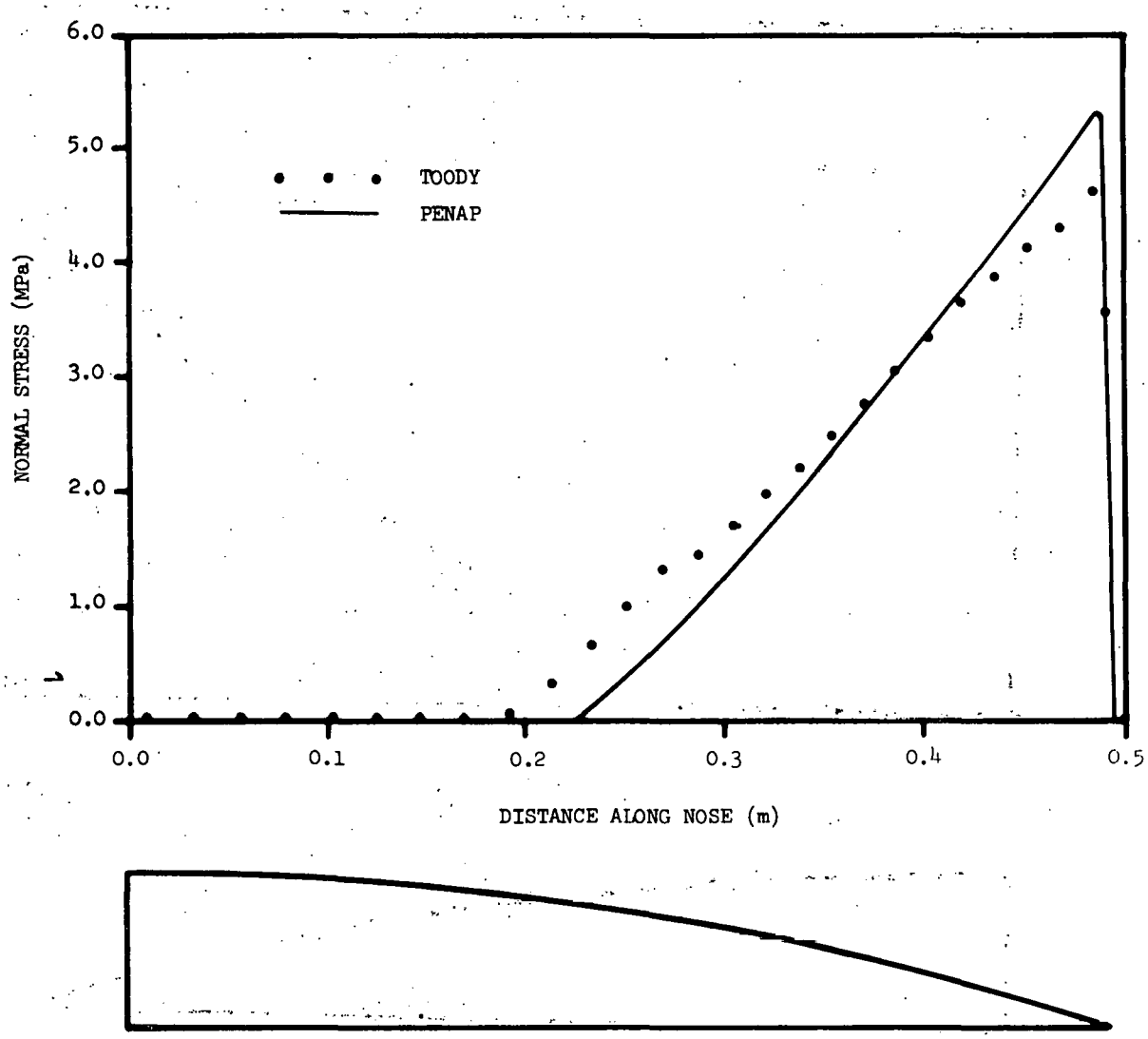

Figure 5. Normal Stress Distribution on Ogival-Nosed Penetrator (Target: Layer 3; Impact Velocity: 75 m/s)

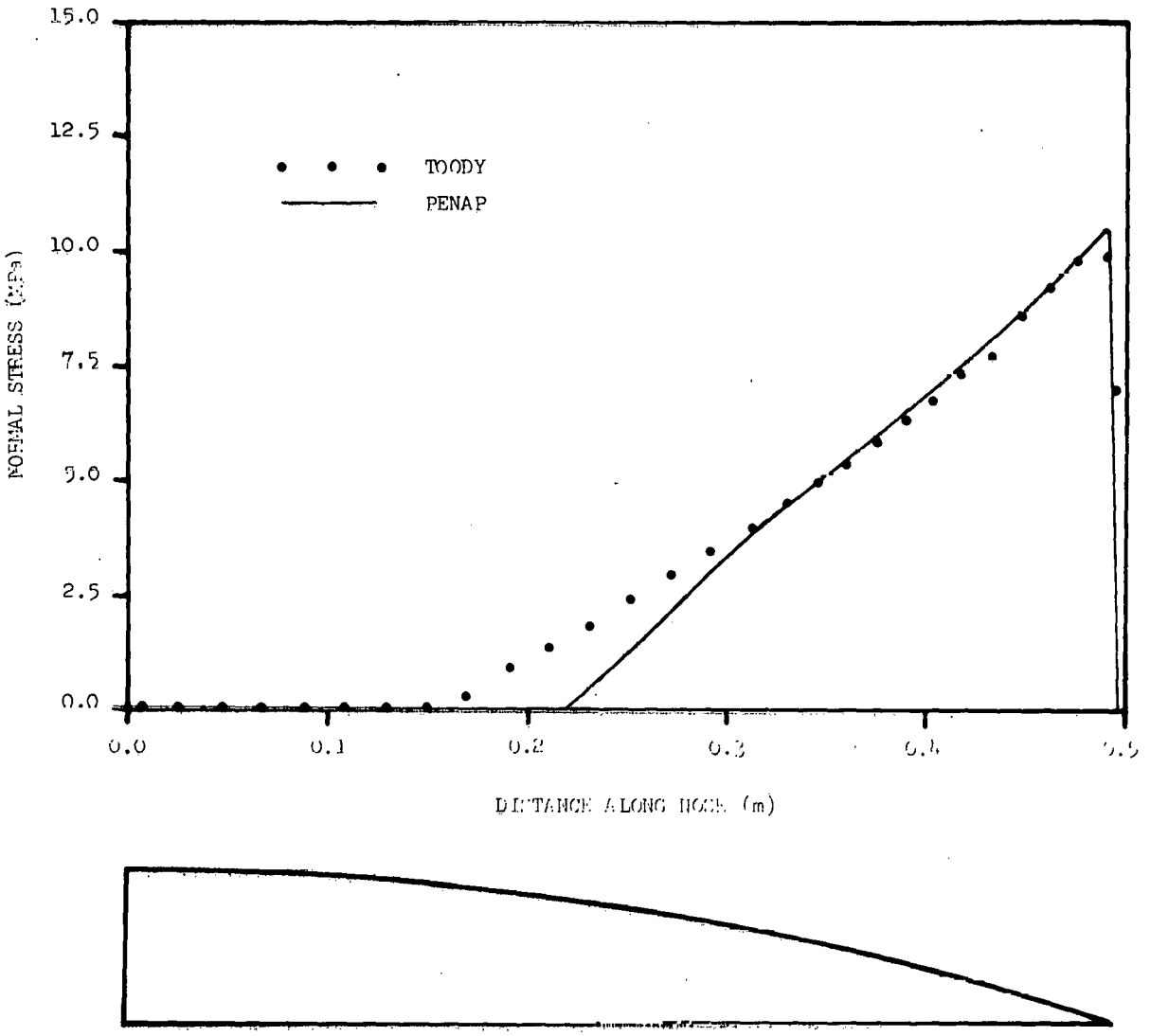

Figure 6. Normal Stress Distribution on Ogival-Nosed Penetrator (Target: Layer 3; Impact Velocity: 150 m/s)

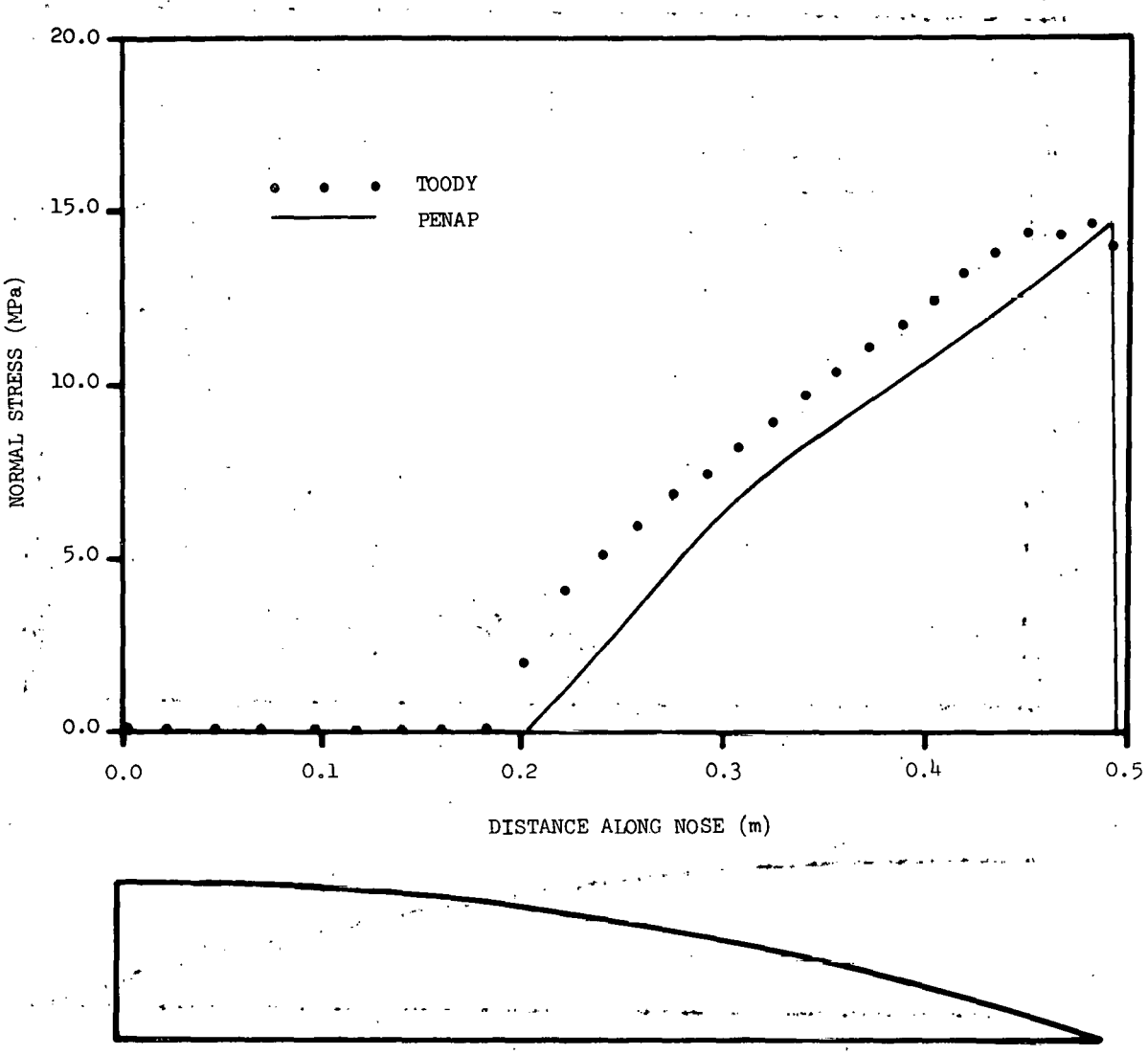

Figure 7. Normal Stress Distribution on Ogival-Nosed Penetrator (Target: Layer 1; Impact Velocity: 150 m/s)

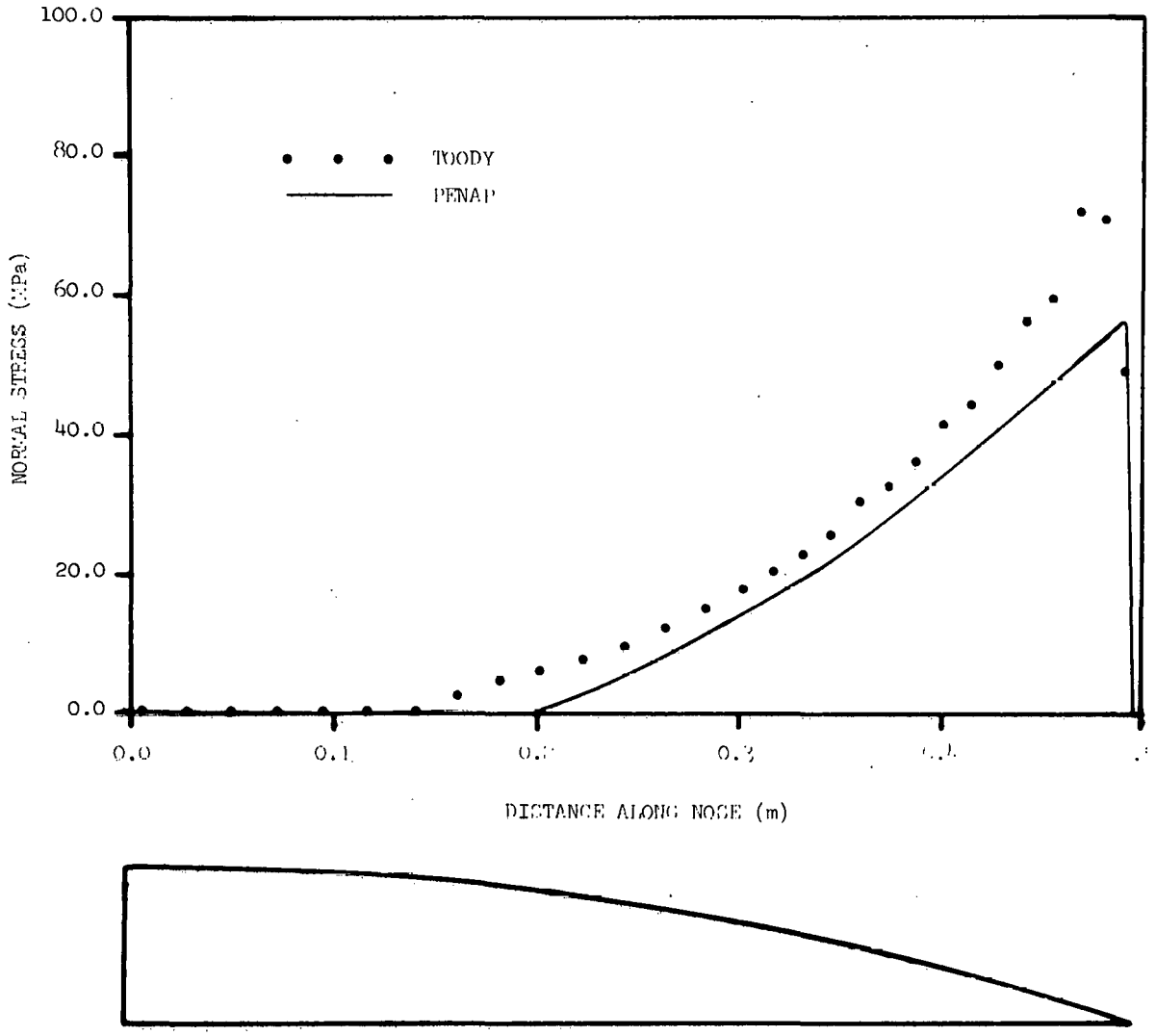

Figure 8. Normal Stress Distribution on Ogival-Nosed Penetrator (Target: Layer 1; Impact Velocity: 500 m/s)

However, it should be noted that in the high velocity results shown for Layer 1 (i.e., Fig. 8), the volumetric strain calculated at the nose tip using the approximate method was about 0.45. At this strain level, pressures obtained from the approximate fit to the hydrostat will lie below those calculated from the cap model. This probably leads to the difference between the stresses calculated at the nosetip.

It should also be noted that the failure surface used for the PENAP calculations is such that the strength of the soil goes to zero with the confining pressure. However, with the cap model the soil has a small but finite strength at zero pressure. This difference between the two models could explain the somewhat higher stresses seen in the TOODY calculations near the back of the nose.

Furthermore, the fact that, for all but very low confining pressures, the linear portion of the curve used to approximate the failure surface lies above the cap-model surface could cause the approximate method to overpredict the stress in the region. This is felt to be the case, for instance, near the nosetip for the calculations compared in Fig. 5.

b. Deceleration Profile for the Watching Hill Experiment

Deceleration data from one test in the Watching Hill series will be used for comparison with calculations. The penetrator for that test was a 0.165 m diameter, 9.25 caliber ogival-nosed projectile, with a mass of 181.44 kg and an impact velocity of 152.4 m/s.

For earlier comparison with TOODY predictions [12] the soil profile at the Watching Hill site was modelled as four distinct, laterally uniform layers. Each of the first three layers was taken to be 2.4 m thick, while

the fourth was assumed to be sufficiently thick to exceed the final depth of penetration for all tests. However, comparison of the calculated and observed deceleration histories strongly suggested that the available quasi-static data for the fourth layer did not accurately represent the target material at that depth. Thus, only results for the first three layers will be used for comparison here.

Figure 9 compares the deceleration data and TOODY predictions taken from [12] with PENAP results for this test. For the approximate solution, the decelerations were assumed to be constant through a given layer, with a magnitude determined by the velocity of the penetrator as it entered the layer.

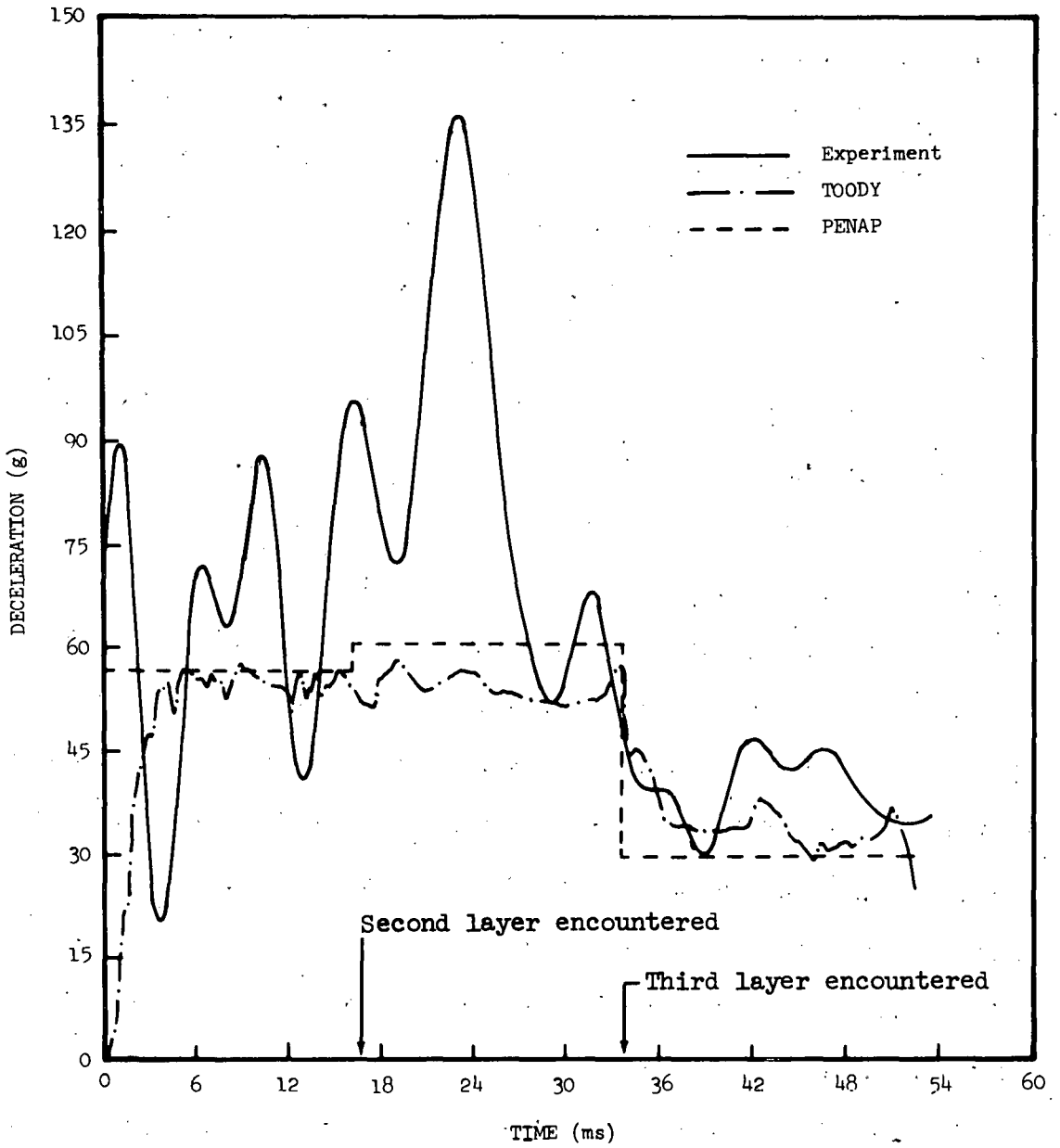

Figure 9. Deceleration History for Penetration of First Three Layers at Watching Hill Site
(Penetrator: 9.25 CRH; Impact Velocity: 150.4 m/s)

VII. CONCLUSION

The one-dimensional approximate technique which was developed here provides a relatively quick method for calculating the normal stress distribution on, and deceleration of, earth penetrators. Particularly attractive about the present method is the use of fairly simple linear and/or quadratic forms for modeling the constitutive response of the target material.

For conical-nosed penetrators an analytic expression was derived for calculating the (spatially constant) normal stress. However, for ogival-nosed penetrators, the equations of the theory must be solved numerically, and an interactive computer program, PENAP, was written for that purpose. Normal stress distributions calculated with PENAP were seen to provide an acceptable approximation to TOODY results for two distinct soil targets and over a fairly wide range of impact velocities. Furthermore, the PENAP calculations required several orders of magnitude less computer time than did the TOODY calculations. It should also be noted that the interactive nature of the PENAP code and the simplicity of the constitution model used in the approximate analysis make problem setup for PENAP considerably easier than for TOODY.

Finally, the deceleration history for one test in the Watching Hill series was calculated using the approximate method. The results showed good agreement with TOODY calculations and were in qualitative agreement with the experimental record for that test.

References

1. Yarrington, P. and N. Ruiz, "PENAP-An Interactive Computer Program for Approximate Calculations of Surface Loads on Earth Penetrators," Report SAND77-1359, Sandia Laboratories, (to be published).
2. Berthoif, L. D. and S. E. Benzley, "TOODY II, A Computer Program for Two-Dimensional Wave Propagation," Report SC-RR-68-41, Sandia Laboratories, November 1968.
3. Thorne, B. J. and D. B. Holdridge, "The TOOREZ Lagrangian Rezoning Code," Report SLA-73-1057, Sandia Laboratories, April 1974.
4. Nelson, I., M. L. Baron and I. Sandler, "Mathematical Models for Geological Materials for Wave-Propagation Studies," Shock Waves and the Mechanical Properties of Solids, Syracuse University Press, Syracuse, New York, Editors: J. J. Burke and V. Weiss, 1971.
5. Lauson, H. S. and R. K. Byers, "The SLA Cap Models and the CAPMOD Code," Report SAND77-1364, Sandia Laboratories (to be published).
6. Yarrington, P., "Comparison of Calculations of Rigid and Deformable Projectiles Penetrating Soil," Report SAND76-0656, Sandia Laboratories, February 1977.
7. Cristescu, N., "Dynamic Plasticity," 1967.
8. Prager, W., "On Ideal Locking Materials," Transactions of the Society of Rheology, Vol. 1, 1957, pp. 169-175.
9. Ross, B. and S. Hanagud, "Penetration Studies of Ice with Application to Arctic and Subarctic Warfare," final report, Project NWCR 7000-452-4, September 1969, Menlo Park, CA (SRI Project 7000-452).
10. Norwood, F. R. "Cylindrical Cavity Expansion in a Locking Soil," Report SLA-74-0201, July 1974.

11. Isenberg, J., "Nuclear Geoplosics," DNA 1285HZ, November 1972.

12. Byers, R. K. and A. J. Chabai, "Penetration Calculations and Measurements for a Layered Soil Target," International Journal for Numerical and Analytical Methods in Geomechanics, Vol. 1, 1977.

DISTRIBUTION

Picatinny Arsenal (4)
Dover, New Jersen 07081
Attn: P. Harris
E. Zimpo
A. Garcia
Technical Library

U. S. Army Advanced Ballastic
Missile Defense Agency (2)
Huntsville Office
P. O. Box 1500
Huntsville, Alabama 35807
Attn: CRDABH-S
CRDABH-X

University of California (3)
Lawrence Livermore Laboratory
P. O. Box 808
Livermore, CA 94550
Attn: Technical Library
M. Wilkins
G. L. Goudreau

Los Alamos Scientific Laboratory
P. O. Box 1663
Los Alamos, NM 87544
Attn: Reports Library

Department of Aerospace Engineering
and Engineering Mechanics
University of Texas
Austin, Texas 78712
ATTN: Prof. C. H. Yew

Atomic Weapons Research Establishment
Aldermaston
Berkshire, England
Attn: B. D. Lambourn

California Research and Technology,
Inc.,
6269 Variel Avenue, Suite 200
Woodland Hills, CA 91364
Attn: K. Kreyenhagen
Technical Library (2)

R. & D. Associates (6)
P. O. Box 2580
Santa Monica, CA 90403
Attn: H. Brode
H. Cooper
C. Knowles
J. Lewis
W. Wright
Technical Library

Science Applications, Inc., (3)
1250 Prospect Street
La Jolla, CA 92037
Attn: D. Maxwell
D. Bernstein
Technical Library

U. S. Army Engineer Waterways
Experiment Station (4)
Soils and Pavements Laboratory
Vicksburg, MS 39180
Attn: G. Jackson
P. Hadala
B. Rohani
Technical Library

Avco Corporation (4)
Research and Systems Group
201 Lowell Street
Wilmington, MA 01887
Attn: D. Henderson
J. Atanasoff
F. Lasher
Research Library - A830,
Room 217

Martin Marietta Aerospace (4)
Orlando Division
P. O. Box 5837
Orlando, FL 32805
Attn: N. Singletory
A. Gowan
M. Anthony
Technical Library

Stanford Research Institute (3)
333 Ravenswood
Menlo Park, CA 94025
Attn: G. Abrahamson
SRI Library, Rm. G021
L. Seaman

DISTRIBUTION (Cont'd)

Physics International Company (4)
2700 Merced Street
San Leandro, CA 94577
Attn: D. Orphal
R. Swift
C. Godfrey
Technical Library

Systems, Science, and Software, Inc., (3)
P. O. Box 1620
La Jolla, CA 92037
Attn: E. Gaffney
D. Grine
Technical Library

Terra Tek, Inc., (3)
University Research Park
420 Wakara Way
Salt Lake City, Utah 84108
Attn: S. Green
A. Jones
Technical Library

Texas A. & M. University
College Station, Texas 77843
Attn: J. Handin

Washington State Univ
Department of Physics
Pullman, Washington 99164
Attn: G. Duvall

Weidlinger Associates, Consulting Engineers (2)
110 E. 59th Street
New York, NY 10022
Attn: J. Wright
M. Baron

A. F. Armament Laboratory, AFSC (3)
Eglin AFB, Florida 32542
Attn: J. Collins
J. Osborne
Technical Library

A. F. Weapons Laboratory, AFSC (2)
Albuquerque, NM
Attn: M. Plamondon
SUL

Pacifica Technology
P. O. Box 148
Del Mar, CA 92014
Attn: R. L. Bjork

Department of Materials Eng'g
University of Illinois at Chicago
Chicago, IL 60680
Attn: T. B. Belytscho

Defense Nuclear Agency (3)
Headquarters DNA
Washington, DC
Attn: STTL
DDST
SPSS

Naval Surface Weapons Center (4)
Dahlgren Laboratory
Dahlgren, VA 22448
Attn: M. Weiland
T. Williams
W. Wisherd
Technical Library

U. S. Energy Research & Dev. Adm.,
Division of Military Application
Washington, D. C. 20545
Attn: Library

University of New Mexico (2)
Albuquerque, New Mexico 87106
Attn: G. Triandafelidis
H. Southward

U. S. Army Ballistic Res. Lab. (2)
Aberdeen Proving Ground, MD 21005
Attn: Technical Library
E. Baicy

Massachusetts Institute of Tech.
Dept of Earth & Planetary Sciences
Cambridge, MA 02139
Attn: W. Brace

Penetrator Study Team
Theoretical and Planetory Studies Branch
Ames Research Center
Moffett Field, CA 94035
Attn: Maxwell B. Blanchard

DISTRIBUTION (Cont'd)

Mail Stop 183B-365
Jet Propulsion Laboratory
4800 Oak Grove Drive
Pasadena, CA 91103
Attn: Geoffrey Briggs

Division of Earth and Planetary
Sciences
California Institute of Technology
Pasadena, CA 91025
Attn: Dr. J. G. Wasserburg

Planetology Programs Manager
NASA Headquarters
Washington, DC 20546
Attn: D. H. Herman

Science Applications Incorporated
5005 Newport Drive, Suite 305
Rolling Meadows, IL 60008
Attn: John Niehoff

DISTRIBUTION (Cont'd)

1281 D. B. Longcope
1284 P. P. Stirbis
1284 W. F. Hartman
1325 W. J. Patterson
1325 C. W. Young
1325 E. W. Reece
4340 H. W. Schmitt
4342 W. R. Reynolds
4342 D. L. McCoy
4360 E. E. Ives
4361 W. C. Hines
5000 A. Narath
Attn: E. H. Beckner - 5200
A. W. Snyder - 5400
J. H. Scott - 5700
R. S. Claassen - 5800
5100 J. K. Galt
Attn: F. L. Vook - 5110
G. J. Simmons - 5120
G. A. Samara - 5130
J. E. Schirber - 5150
5160 W. Herrmann
5162 L. D. Bertholf
5162 M. E. Kipp
5163 D. E. Munson
5163 D. Grady
5166 A. J. Chabai
5166 S. L. Thompson
5166 R. K. Byers
5166 N. K. Ruiz
5166 P. Yarrington (30)
5166 W. R. Davey
5166 F. R. Norwood
5444 D. R. Anderson
5444 D. M. Talbert
8120 W. E. Alzheimer
8266 Technical Library (2)
8360 J. F. Barham
3141 Technical Library (5)
3151 Technical Library (3)
for ERDA/TIC (Unlimited Release
ERDA/TIC (25)
(3171-1 R. P. Campbell)